J. Condensed Matter Nucl. Sci. 33 (2020) 168–193

Research Article

Condensed Plasmoids (CPs) – A Quantum-Mechanical Model of the Nuclear Active Environment of LENR

Lutz Jaitner*

85405 Nandlstadt, Germany

Abstract

Researchers have long been puzzled about the basic nuclear reaction mechanisms of low-energy nuclear reactions (LENR). Usually the crystal lattice or nano-particles (among others) are assumed to be the nuclear active environment that catalyzes the reaction somehow. In contrast, the author has built a quantum-mechanical model of the nuclear active environment in LENR, where this environment is modeled as an ultra-dense plasmoid, i.e. a "condensed plasmoid" (CP). The computed properties of CPs are so exotic that CPs qualify as a previously unknown aggregation state of matter. The quantum-mechanical model of CPs is based on the cylindrical symmetry of a very thin (i.e. about 40 pm) plasma "wire". (The quantitative properties given in the abstract depend on the configuration of the CP; these are just examples.) The electrons of a CP are fully delocalized and decoupled from the nuclei. They are moving with high velocity (10–80% of light speed) against the nuclei. This results in an intrinsic current of about 9 kA in the CP with a mean current density of approximately 2.5 A/pm^2. The magnetic field from this current reaches 50 MT (magatesla) and creates a confinement pressure of more than 10^{21} Pa. The electrons are compressed by the strong z-pinch condition to a mean density of about 0.15 electrons/pm^3. The creation of a CP is an endothermic process (i.e. it takes in energy from an external source), which typically requires discharges with high voltages and high currents. Once created, these objects can be long-living (lasting hours). The minimum distance of hydrogen nuclei in a CP is only about 2 pm, which enables tunneling of nuclei through the Coulomb barrier, i.e. nuclear fusion. The barrier is also much screened by the dense electrons.
 ISSN 2227-3123

Keywords: Charge clusters, EVs, EVOs, LENR, Nuclear active environment, Pease-–Braginskii current, Plasmoids, Rradiative collapse, Strange radiation, z-Pinch

1. General Description

This article is an extract from a much more comprehensive document on the author's web site [1]. The term "condensed plasmoid" was recently coined, and is presented in this document for the first time, thus a definition is given here. A CP is defined to be a plasmoid (i.e. a self-consistent structure of a current-carrying plasma and magnetic fields), which meets all of the following criteria.

*Web: www.condensed-plasmoids.com. E-mail: lutz.jaitner@t-online.de.

 ISSN 2227-3123

- The plasmoid is compressed by a strong z-pinch condition. "Strong" in this sense means that the internal current is larger than 200 A; the radius of the plasma channel is less than 200 pm; and the length of the plasma channel is at least several micrometers. These numbers are based on the computational results of the current modeling. For yet unknown reasons CPs might exist with lower intrinsic currents.
- All electrons of the containing atoms (not merely the outer electron shells) are delocalized, i.e. the electrons are all contributing to the current and they can freely move between the atomic nuclei. The delocalization is caused by the small inter-nucleic distance (i.e. less than 10 pm in case of hydrogen).
- The electrons reside in orbitals, which are at (or near) the quantum-mechanical ground state of the CP. For this to be true, the temperature of the CP must be low enough that the thermal pressure of the plasma is smaller than the magnetic pressure enforced on the moving electron gas by the Lorentz force.

A direct consequence of this definition is that CPs are representing mesoscopic objects of matter. "Mesoscopic" means "in between quantum-mechanical and macroscopic". The properties of CPs therefore do not always follow the conventional wisdom of plasma physics. For example, cooling down a CP will not produce electron-ion recombinations and ordinary molecules.

CPs exist in different topologies.

- The open-ended configuration of a CP exists under transient conditions in the presence of a strong electric field. An open-ended CP loses electrons at the negative end. The positive end of an open-ended CP is often connected to a cathode, which replaces the electrons lost at the other end.
- The closed-loop configuration of a CP is the long-lasting form, where the internal current is flowing in a circular manner. Closed-loop CPs can exist even in the absence of an external electric field. Based on the microscopic evidence, there are various mechanisms by which closed-loop CPs can develop. These mechanisms are typically supported by the electrostatic attraction between the electrons and the cations. The positive and negative charges will rapidly find a path to meet if the loop is not yet closed. Along this path the plasmoid then condenses. Another mechanism would be, if a CP is spawning a closed loop by overlapping with itself.

Imprints of CPs have been observed in LENR experiments both at the surface of cathodes and as images on x-ray films or nuclear emulsions. In the latter case CPs were emitted by LENR experiments (sometimes called "strange radiation"), which exposed the films/emulsions.

Imprints of ring-shaped CPs have been documented by different research groups in the following images (Fig. 1):

The primary structure of CPs has a cylindrical shape, i.e. it is a plasma "wire", which is long, very thin and rotational symmetric. Most, but not all, properties of CPs can be derived from the cylindrical structure. At longer

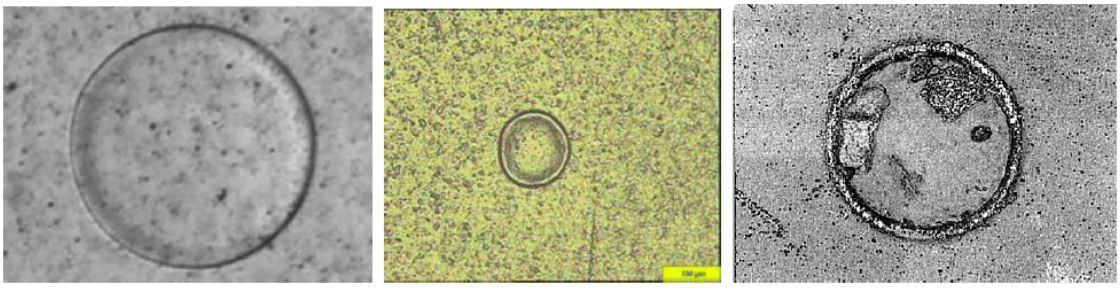

Figure 1. CP rings on X-ray film, diameter $= 0.2$ mm by Claude Daviau et al. [2] (*left*) and by B. Rodinov and I. Savvatimova [3] (*middle*). CP ring on an electrode by T. Matsumoto [4] (*right*).

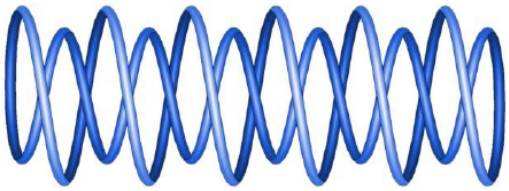

Figure 2. Drawing of a CP coiling up in a two-layered closed-loop solenoid via magnetic self-interaction.

CPs the ultra-strong magnetic field of CPs is deforming the plasma-wire, leading to a secondary structure, i.e. CPs are tending to coil up in two-layered closed-loop solenoids is shown in Fig. 2.

Imprints of the helical secondary structure of CPs were documented by B. Rodinov and I. Savvatimova (Fig. 3). CPs can create significant erosion craters at the cathode (Fig. 4): The author believes that the patterns left by CPs are not merely a strange side effect of LENR, but they provide the experimental core evidence of the presence of CPs in such experiments. The term "nuclear-active environment" has been coined by Edmund Storms [7] in an attempt to characterize the properties of the zone where the nuclear reactions of LENR actually happen. Taking this concept

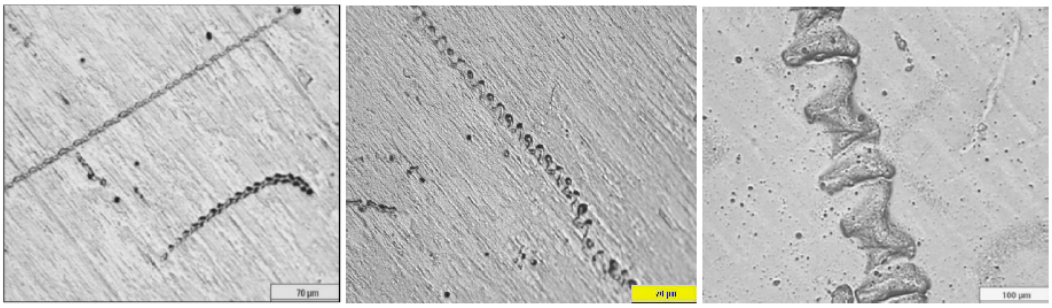

Figure 3. Quasi-periodic patterns from helical CPs produced by glow discharge. *Left and middle*: Pd cathode, *right*: nuclear emulsion [3].

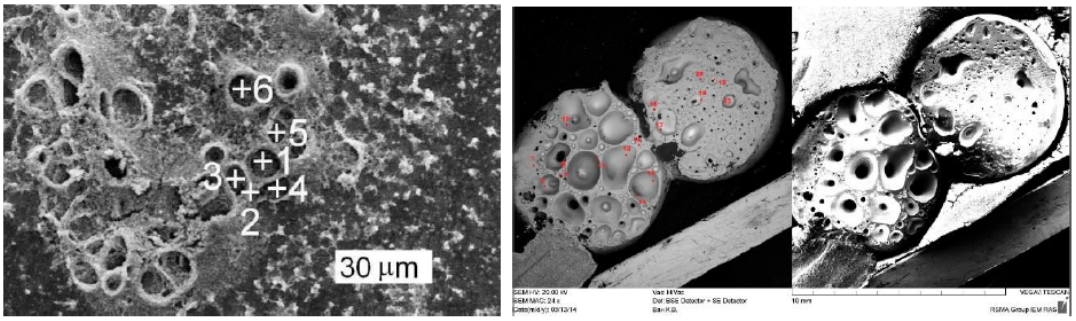

Figure 4. Volcano-like structures at the palladium cathode surface after electrolysis of heavy water, W.-S. Zhang and J. Dash [5] (*left*); Erosion craters in the nickel cathode of the plasma vortex reactor of A. Klimov et al. [6] (*right*).

to the next step, the nuclear active environment is equated here with CPs. Without CPs there can be no excess heat, because the nuclei can fuse only in the dense environment of CPs.

The main idea of this theory on CPs is as follows. The azimuthal component of the magnetic field at the surface of a plasma wire is inversely proportional to the radius of the conducting channel (and proportional to the CPs intrinsic current). Therefore, the more the magnetic field compresses the plasmoid, the stronger the magnetic field becomes and the stronger the plasmoid is compressed. It is a *positive feedback mechanism*: When the current divided by the plasmoid radius increases beyond a critical threshold, there will be a rapid compression of the plasmoid ("condensation").

However, not all plasmoids will readily condense. For example, an electric arc is often too hot and the ionized channel is often too wide for the condensation to take place. The continuing current heats the plasmoid by resistive losses, which negatively affects the ability of the plasmoid to condense.

If the temperature is kept low enough, only the degeneracy pressure of the electron gas will hinder a total collapse of the matter. The degeneracy pressure is a quantum-mechanical result of the Pauli Exclusion Principle. It increases with increasing electron density.

A quantum-mechanical model of CPs had to be established in order to compute the equilibrium radius (and other properties) of CPs. (This refers to the equilibrium between the magnetic pressure and the quantum-mechanical pressure of the electron gas.) The scope of the model is to describe the stationary state after the compression of the plasmoid, rather than modeling the dynamic aspects of the compression.

During condensation the matter density increases dramatically and the scattering probability of the electrons decreases to almost zero. Electron scattering in CPs differs from electron scattering in ordinary plasmoids by the fact that most of the lower-energy orbitals of CPs are already occupied and there is no energy available for scattering electrons into higher-energy orbitals. As a result, the resistance of the CP drops to levels very close to zero (a phenomenon not necessarily related to superconductivity), and the current in a close-looped CP can flow for a very long time.

There is a minimum length of a CP, which is believed to be a few micrometers. Based on this length, CPs contain at least a hundred million electrons. There is no maximum length, i.e. CPs can be made arbitrarily long.

W.H. Bennett in 1934 [8] showed that there is an equilibrium between the thermal pressure of a plasma channel and the magnetic pressure of a pinched plasmoid, if the so called Bennett relation is met:

$$k_{\mathrm{B}}\left(N_{\mathrm{e}}T_{\mathrm{e}}+N_{\mathrm{i}}T_{\mathrm{i}}\right)=\frac{\mu_0}{4\pi}I^2, \tag{1}$$

where N_{e} is the number of electrons per unit length of the plasma channel, N_{i} the number of ions per unit length of the plasma channel, I the total current, μ_0 the vacuum permeability, k_{B} the Boltzmann's constant, T_{e} the electron temperature and T_{i} is the ion temperature.

This relation assumes that the velocity distribution of the electrons and ions obey the Boltzmann statistics of an ideal gas. This assumption is invalid in the case of CPs, because their plasma is fully degenerate (Fermi gas) and the temperature is low.

The possibility of radiative collapse in pinched linear discharges was first studied independently by Pease [9] and Braginskii [10,11] in 1957 for pure hydrogen or deuterium plasmas. When radiation losses by bremsstrahlung exceed Ohmic heating at high currents, they predicted shrinking of the plasma channel, which may even result in a collapse of the channel to extremely high densities. They derived a critical current value (i.e. the Pease–Braginskii current) that has to be exceeded to achieve a collapse:

$$\frac{I_{\mathrm{PB}}}{\mathrm{MA}}\approx 0.27\sqrt{\ln\Lambda}\left(1+\frac{1}{Z}\right), \tag{2}$$

where $\ln\Lambda$ is the Coulomb logarithm, MA stand for megaampere and Z is the charge of the ions.

Formula (2) is assuming an infinitely long plasma channel and $T_{\mathrm{e}}=T_{\mathrm{i}}$. It is based on Spitzer resistivity (first formulated by Lyman Spitzer [12] in 1950), where the resistivity of the plasma channel is proportional to $T_{\mathrm{e}}^{-3/2}$.

There were many later attempts in the literature to refine the original formula of Pease and Braginskii, but the issues at low temperatures were not addressed, as far as the author is aware of.

Spitzer resistivity is built upon classical electron–ion collisions (this can be seen as a high-temperature approximation), whereas at low temperatures the scattering behavior of the electrons can only be understood by a quantum-mechanical analysis. With Spitzer resistivity one would conclude that the plasma channel becomes non-conductive (and Ohmic losses would diverge) when the temperature approaches zero. In reality the resistivity of a CP is lowest at the lowest temperatures. The physical reason for this discrepancy is that electron–ion scattering is energetically hindered at low temperatures in CPs. Instead the resistivity of a CP is mainly based on electron–phonon scattering, which also becomes negligible at very low temperatures.

Also, the Pease–Braginskii formula merely considers Bremsstrahlung as the cooling mechanism, where in reality line radiation of heavier atoms, heat transport by delocalized electrons, stimulated cyclotron radiation, and direct thermal conduction to the environment contribute to the cooling during the condensation phase.

The Pease–Braginskii current is typically computed as being in the order of 1.5 MA for hydrogen. It decreases to about 100 kA for elements like Ar, Kr and Xe, because line radiation dominates over Bremsstrahlung and the radiative cooling thus becomes more efficient.

With peak currents in the range of 150–200 kA evidence for radiative collapse has been found [13]: Low-inductance vacuum sparks produced by discharging a capacitance of 10–30 μF (charged to 10–20 kV) through a circuit inductance of 50–100 nH achieves pulse lengths of 1.5–2 μs. The sparks are producing small, point-like regions in the plasma that are called plasma points, bright spots, or hot spots. (Similar observations have been made in plasma focus devices and in gas puffs.)

The first phase of the discharge creates a plasma with material eroded from the electrodes. In the next phase of the discharge the current increases as prescribed by the electrode voltage and the inductance of the circuit. On top of the smoothly rising current there appear short (<100 ns) single or multiple dips in the current. These current dips are accompanied by intense bursts of X-rays with photon energies of 5–150 keV. The current dips are correlated with the appearance of plasma points. The points are often less than 10 μm in size.

It is remarkable that the maximum X-ray photon energy is much higher than the theoretical maximum energy of the electrons traversing the electric field between the electrodes. The maximum photon energy also exceeds the K-shell energy of the plasma ions. These high photon energies can be explained by electron relaxation in CPs, which have a Fermi energy (i.e. the energy difference between the highest and the lowest occupied orbital) of up to 200 keV.

The observed current dips can be interpreted as the condensation phase of the CPs: When the radius of the CPs is shrinking the magnetic flux of the CPs is compressed. This is electromagnetically inducing a high voltage counter to the externally applied voltage. During the current dips compression work is applied to the CPs by means of the external field. At the end of the compression phase (i.e. the end of the current dip) the current continues to rise and the generated CPs continue to exists, but the electron relaxation is mostly complete and the X-ray emission fades.

The fact that sometimes multiple current dips have been observed during the same discharge can be interpreted to mean that several CPs have been created in parallel, which successively condensed. This could be due to a filamentation instability of the initial plasmoid.

J. Va'vra et al. determined the smallest possible spark current, which is still consistent with the X-ray production and the development of plasma points [14]. Their generator used a spark gap operating at low pressure (0.1–1 Torr) and low discharge voltages between 0.8 and 2.1 kV. The charging capacitance was 75 nF, the circuit inductance was about 1000 nH, the stored energy amounted to 0.024–0.17 J per pulse, the peak spark currents was 200–500 A and the total capacitor charge was between 4×10^{14} and 10^{15} electrons. The spark gap was 1 mm.

The observed X-ray energies were between 2 and 10 keV even at the lowest sparking voltage of about 0.8 kV (depending on the gas). The maximum observed X-ray energy ($\sim$10 keV), generated at the lowest voltage ($\sim$0.8 kV), is above K-shell energy of typical gases used in the tests, and materials used in the spark electrodes. The X-ray

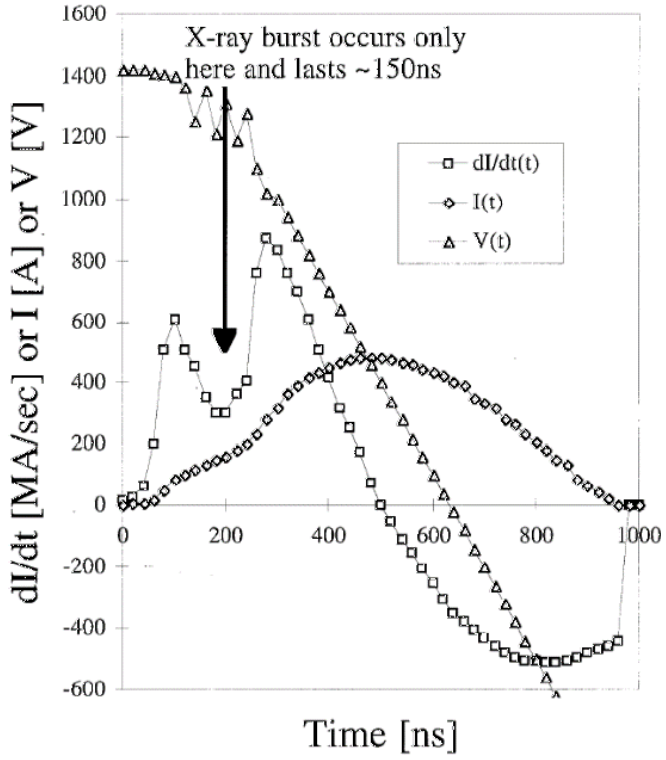

Figure 5. Current and voltage development in a low-pressure spark discharge according to J. Va'vra et al. [14].

production persisted even for the carbon electrodes which have the smallest K-shell energy (0.284 keV). The spark current and the electrode voltage were measured as follows (Fig. 5).

The radiative collapse of the plasmoid (which can be equated with the condensation of a CP) occurred during the dip of the $\mathrm{d}I/\mathrm{d}t(t)$ curve, which lasted about 150 ns. It is very interesting that this collapse occurs already at a current of about 200 A.

2. CP Quantum Mechanics

2.1. Basic assumptions

Modeling of CPs is based on the following basic assumptions:

(a) CPs contain ensembles of atomic nuclei densely packed in a long and very narrow channel.
(b) The distances between the nuclei are so small, that all electrons bound to these nuclei are delocalized along the channel. In other words, even in their electronic ground state CPs do not consist of individual atoms. Instead, CPs form a quasi-one-dimensional plasma (Fig. 6).

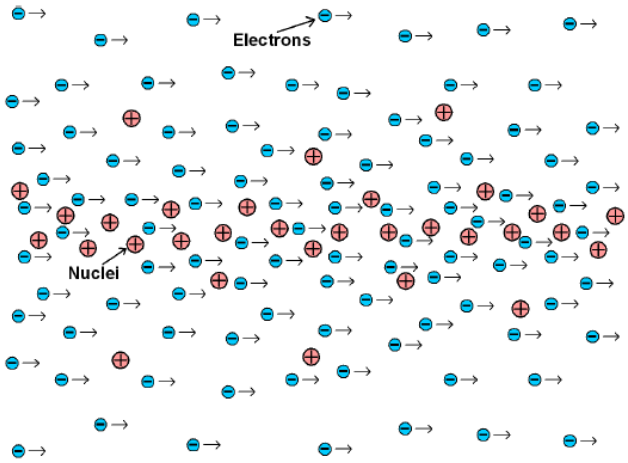

Figure 6. Basic model of a CP. The CP similarly extends to the left and to the right of this picture.

2.2. The cylindrical model of CPs

The shape and quantum mechanical state of CPs can be very complicated. In order to obtain a simple quantum mechanical description of CPs, the following simplifications are used, which will subsequently be called "the cylindrical model of CPs".

(c) The CP is perfectly straight and cylindrically symmetric, i.e. it is not bent to rings, helices, etc. The CP is oriented in parallel to and centered on the $z$axis of the modeling cylindrical coordinate system.
(d) The CP has the length $\bar{L}$ and contains a total nuclear charge Q in its core.
(e) The electron wave functions of the CP are confined in the interval $0 \leq z < \bar{L}$. At $z = \bar{L}$ these wave functions are continuously extended to their value and gradient at $z = 0$, as if the CP were a ring. However, this is meant to describe only the *circular boundary condition* of the wave functions at $z = \bar{L}$, not the shape of the CP.
(f) No external field is applied to the CP.
(g) A *jellium* model is used for the spatial distribution of the nuclear charge. This means, for the purpose of computing the spatial distribution of the electrons, the positive charges of the nuclei are modeled as a uniform "positive jelly" background, rather than point charges with distances in between. The nucleic charge density is assumed to be constant in axial and azimuthal direction, but it depends on the radial distance.
(h) The nucleic charge distribution of the jellium is modeled by means of a two-dimensional distribution function in radial direction. This function is to be determined, such that the total energy of the CP is minimized.
(i) The core area of the CP (i.e. the space defined by the extent of its electron orbitals) is surrounded by a charge compensation layer ("halo") consisting of cations. The charge of the halo compensates the surplus negative charges of the electrons in the core. The halo is modeled as a cylindrical shell of positive charge. The halo radius has to be larger than the core radius.
(j) The CP is assumed to reside in a vacuum. Interaction of the CP with surrounding matter is thus neglected.
(k) Only stationary states are modeled, as the goal is to describe the ground state of a CP. Consequently, the model assumes there is no electron scattering, i.e. there is no momentum transfer between electrons and the nuclei.
(l) The time-independent Klein–Gordon equation is used for modeling the electron wave functions, thereby

neglecting the magnetic moments of electron spins. The Klein–Gordon equation takes care of the sizable relativistic effects occurring in CPs. (Clearly, the Dirac equation would be more adequate for modeling CPs. However, the involved complexities of such approach are avoided here.) For comparing the formulas and simulation results with the ones obtained from a non-relativistic Hamiltonian, also the Schrödinger equation is used.

(m) The magnetic field of the azimuthal electron orbits is neglected.
(n) Magnetic field from nuclear spins is neglected.
(o) The electron wave functions are modeled in an inertial frame of reference, where no magnetic field is created by any collinear movements of the nuclei. This simplification amounts to an approximation in cases where the nucleic velocities are position dependent.
(p) The multi-electron system is approximated by computing a collection of one-electron orbitals, whereby each electron orbital is subjected to the mean electric potential and magnetic vector potential created by the total charge density and total current density of all other occupied orbitals and the nuclei (independent particle model). The Pauli Exclusion Principle is used for determining orbital occupations of the ground state. Exchange and correlation energies are neglected.
(q) Quantum field theory is not engaged. Particle count is conserved.
(r) Eigen states are excluded from occupation, where the corresponding total energy eigenvalue (including the electron's rest energy) of the electron is negative. This shall ensure that the mass defect per electron doesn't exceed the electrons rest energy.
(s) The kinetic energy of the electrons is always positive, i.e. states with a negative kinetic energy are ignored.

2.3. The Klein–Gordon equation of a CP

Initial calculations of a CP with the Schrödinger equation have shown that the spectrum of the axial electron velocities can reach 80% of the speed of light. This provided a reason for engaging a relativistic Hamiltonian and a Lorentz-covariant quantum mechanical equation to model CPs. Assuming that the electron spins have only minor effects on the results, the Klein–Gordon equation was chosen for the modeling instead of the more complicated 4-component Dirac equation.

At the non-relativistic limit the Klein–Gordon equation is equivalent to the Schrödinger equation, which was also used for comparison.

In relativistic electrodynamics with the so-called minimal coupling the Hamiltonian (total energy) of a particle with charge q moving in the presence of a static (external) electromagnetic potential is

$$\hat{H} = c\sqrt{\left(\vec{P} - q\vec{A}\right)^2 + m_{\mathrm{e}}^2 c^2} + q\Phi, \tag{3}$$

where c is the speed of light, Φ the electric potential, $\vec{A}$ the magnetic vector potential, $\vec{P} = \gamma m_{\mathrm{e}}\vec{v} + q\vec{A}$ the electron's canonical momentum, m_{e} the electron rest mass and γ is the Lorentz factor. All formulas are written in SI units, unless otherwise noted.

By quantizing the canonical momentum via the del operator $\vec{P} \equiv -i\hbar\nabla$ and applying both sides to an electron wave function Ψ, Eq. (3) transforms to the *stationary Klein–Gordon equation of an electron in a static electromagnetic potential:*

$$\left(\bar{E} + e\Phi + m_{\mathrm{e}}c^2\right)^2 \Psi = \left[\left(-i\hbar c\nabla + ec\vec{A}\right)^2 + m_{\mathrm{e}}^2 c^4\right]\Psi, \quad \text{where } \bar{E} \equiv \hat{H} - m_{\mathrm{e}}c^2 \tag{4}$$

is the total energy minus the rest energy, $\hbar$ is the reduced Planck constant, e is the elementary charge and $i = \sqrt{-1}$.

Due to simplification (q), Ψ is called here a "wave function", rather than a "quantum field".

The term $\bar{E} + m_{\mathrm{e}}c^2$ represents the total energy of the electron. Usually the Klein–Gordon equation is written such that the total energy is sought as the eigenvalue of this differential equation. However, this document deviates from the customary approach. Instead, the quantity $\bar{E}$ is sought here as the eigenvalue (both approaches are equivalent in their results).

Some authors prefer the term "relativistic Schrödinger equation" for Eq. (4). Here, these terms are used interchangeably. In quantum mechanics a multi-electron system is correctly described by a single wave function $\Psi(\vec{r}_1, \vec{r}_2, ..., \vec{r}_N)$ depending on the positions of the N electrons.

By means of the mean-field approach (assuming the particles are independent) a multi-particle wave function is usually formed as a Hartree product of wave functions:

$$\Psi(\vec{r}_1, \vec{r}_2, ..., \vec{r}_N) = \chi_1(\vec{r}_1) \cdot \chi_1(\vec{r}_2) \cdots \chi_1(\vec{r}_N).$$

In order to take care of the fermionic nature of the electrons one typically has to engage a Slater determinant (or a linear combination of several Slater determinants) to ensure anti-symmetry and the Pauli Exclusion Principle [15]:

$$\Psi(\vec{r}_1, \vec{r}_1, ..., \vec{r}_N) = \frac{1}{\sqrt{N!}} \begin{vmatrix} \chi_1(\vec{r}_1) & \chi_2(\vec{r}_1) & \cdots \chi_N(\vec{r}_1) \\ \chi_1(\vec{r}_2) & \chi_2(\vec{r}_2) & \cdots \chi_1(\vec{r}_2) \\ \vdots & \vdots & \ddots \vdots \\ \chi_1(\vec{r}_N) & \chi_2(\vec{r}_N) & \cdots \chi_1(\vec{r}_N) \end{vmatrix}. \tag{5}$$

According to simplification (p) a rigorously simpler approach is used here for modeling CPs, requiring only moderate computer power:

So, instead of using a multi-electron Klein–Gordon equation describing the pair-wise interaction between N electrons, the cylindrical model uses *N single-electron Klein–Gordon equations with N wave functions* $\Psi(\vec{r})$, each describing a single electron in the *mean potential* of all other electrons and the nuclei. Of course, this is merely an independent particle approximation. For example, the approach does not account for the exchange energy and the correlation energy usually deemed important in quantum chemistry.

At first glance this looks still challenging to compute, because there are N Klein–Gordon equations to be solved. Fortunately, large numbers of these equations can be computed in groups, because they produce nearly the same charge density distributions and current density distributions.

According to simplifications (l) and (k) the magnetic field of the electron spins and of the azimuthal movement of the electrons is neglected. Thus, the only source of the magnetic field is the current carried by the electrons moving in the z-direction. Therefore, the vector potential is everywhere oriented in the z-direction:

$$\vec{A} = \bar{A}_z \vec{e}_z \tag{6}$$

Transforming to cylindrical coordinates, using $\nabla \cdot \vec{A} = 0$ (Lorentz gauge in the static case) and inserting Eq. (6) into Eq. (4) is resulting in *the stationary Klein–Gordon equation of an electron in the mean potential of a CP's all other electrons and the nuclei:*

$$\left\{\frac{-\hbar^2}{2m_\mathrm{e}}\left[\frac{1}{\rho}\frac{\partial}{\partial\rho}\left(\rho\frac{\partial}{\partial\rho}\right)+\frac{1}{\rho^2}\frac{\partial^2}{\partial\phi^2}+\frac{\partial^2}{\partial z^2}+2\frac{e\bar{A}_z}{\hbar}i\frac{\partial}{\partial z}-\frac{e^2\bar{A}_z^2}{\hbar^2}\right]\right.$$
$$\left.-\frac{m_\mathrm{e}c^2}{2}\left(\frac{\bar{E}+e\Phi}{m_\mathrm{e}c^2}+1\right)^2+\frac{m_\mathrm{e}c^2}{2}\right\}\Psi=0, \tag{7}$$

where ρ is the radial distance from the z-axis, φ is the azimuth and z is the coordinate of the z-axis.

With simplification (f) the electric potential Φ is depending solely on the electron charge density $\bar{\sigma}_\mathrm{e}(\rho)$ and the nuclear charge density $\bar{\sigma}_\mathrm{n}(\rho)$. The magnetic vector potential $\bar{A}_z$ is solely dependent on the electric current density $\bar{J}_z(\rho)$. The electron charge density and the electric current density are derived from the modulus square of the other electron's wave functions. This approach has *similarities with the density functional theory (DFT)* used in quantum chemistry modeling, except that the exchange and correlation energies are not accounted for. Equation (7) therefore can be seen as the Kohn–Sham equation [16].

2.4. Boundary conditions for solutions of the Klein–Gordon equation

Care must be taken according to simplification (r), that *the total energy $\bar{E}+m_\mathrm{e}c^2$ of an eigenstate is always positive*, therefore:

$$\bar{E}>-m_\mathrm{e}c^2. \tag{8}$$

Requirement (8) can be fulfilled by *excluding eigenstates with a negative total energy during orbital occupation*. The wave function amplitude must disappear at infinite radial distances:

$$\lim_{\rho\to\infty}\Psi(\rho)=0. \tag{9}$$

As required by simplification (e) the wave function has to meet circular boundary conditions:

$$\Psi(z=0)=\Psi\left(z=\bar{L}\right)\quad\text{and}\quad\frac{\partial\Psi(z=0)}{\partial z}=\frac{\partial\Psi\left(z=\bar{L}\right)}{\partial z}. \tag{10}$$

For computing observables the Klein–Gordon electron wave functions have to be *normalized* such that:

$$1=\|\Psi\|=\iiint_{\mathbf{R}^3}|\Psi|^2\mathrm{d}\vec{r}. \tag{11}$$

2.5. Observables of the Klein–Gordon electron wave function

The potential energy of an electron is solely stemming from the Coulomb field:

$$\bar{E}_\mathrm{pot}(\vec{r})=-e\Phi(\vec{r}). \tag{12}$$

The local kinetic energy of the electron is what's left when the potential energy is subtracted from $\bar{E}$:

$$\bar{E}_\mathrm{kin}(\vec{r})=\bar{E}+e\Phi(\vec{r}). \tag{13}$$

By using modulus square factorization (31) the *volume charge density distribution* of all Nelectrons of the CP computes as

$$\bar{\sigma}_{\mathrm{e}} = -e\sum_{i=1}^{N}|\Psi_i|^2 = -\frac{e}{2\pi\bar{L}}\sum_{i=1}^{N}|\Psi_{\rho,i}|^2, \tag{14}$$

where $\Psi_{\rho,i}$ is the radial wave function of electron number i

The *current density distribution* of all N electrons of the CP is

$$\vec{\bar{J}} = \frac{-e}{m_{\mathrm{e}}}\sum_{i=1}^{N}\left[-\frac{i\hbar}{2}\left(\Psi_i^*\nabla\Psi_i - \Psi_i\nabla\Psi_i^*\right) + e\vec{A}\,|\Psi_i|^2\right]. \tag{15}$$

Using product ansatz (29), modulus square factorization (31) and Ψ_z-solution (33), the *z-component* (in cylindrical coordinates) *of the current density* (15) in a CP computes as

$$\bar{J}_z = \frac{-e}{m_{\mathrm{e}}}\sum_{i=1}^{N}\left[-\frac{i\hbar}{2}\left(\Psi_i^*\frac{\partial\Psi_i}{\partial z} - \Psi_i\frac{\partial\Psi_i^*}{\partial z}\right) + e\bar{A}_z\,|\Psi_i|^2\right] = \frac{-e}{2\pi m_{\mathrm{e}}\bar{L}}\sum_{i=1}^{N}\bar{p}_{z,i}\,|\Psi_{\rho,i}|^2, \tag{16}$$

where

$$\bar{p}_{z,i} = \bar{P}_{z,i} + e\bar{A}_z = \hbar k_i + e\bar{A}_z \tag{17}$$

is *the z-component of the electron's kinetic momentum* $\hat{p}$.

The total *current* in z-direction carried by all electrons of the CP can be computed by integrating (16) over all radius values and azimuth values:

$$\begin{aligned} I_z &= \int_{\phi=0}^{2\pi}\int_{\rho=0}^{\infty}\bar{J}_z(\rho)\,\rho\,\mathrm{d}\rho\,\mathrm{d}\phi = \frac{-e}{m_{\mathrm{e}}\bar{L}}\int_0^{\infty}\sum_{i=1}^{N}\bar{p}_{z,i}\,|\Psi_{\rho,i}(\rho)|^2\rho\,\mathrm{d}\rho \\ &= \frac{-e}{m_{\mathrm{e}}\bar{L}}\sum_{i=1}^{N}\int_0^{\infty}\left[\hbar k_i + e\bar{A}_z(\rho)\right]|\Psi_{\rho,i}(\rho)|^2\,\rho\,\mathrm{d}\rho, \end{aligned} \tag{18}$$

The expectation value of the *electron group velocity's z-component* (averaged over all N electrons of the CP) can be computed from the z-component of the total current:

$$\langle v_z\rangle = \frac{I_z\bar{L}}{-Ne}. \tag{19}$$

The *expectation value of the electron orbit radius* for eigenstates of Eq. (7) is

$$\langle\rho\rangle = \int_0^{\infty}|\Psi|^2\,\rho^2\mathrm{d}\rho. \tag{20}$$

The *total formation energy* $\bar{E}_{\mathrm{B}}$ of a CP is

$$\bar{E}_{\mathrm{B}} = \bar{E}_{\mathrm{n}} + \sum_{i=1}^{N}\left(\bar{E}_i - \frac{1}{2}\left\langle\bar{E}_{\mathrm{C,e}}\right\rangle_i\right), \tag{21}$$

where $\bar{E}_{\mathrm{B}}$ is the nuclear repulsion energy defined in (40), $\left\langle\bar{E}_{\mathrm{C,e}}\right\rangle_i = \langle -e\Phi_{\mathrm{e}}\rangle_i$ is the expectation value of the electron–electron Coulomb energy for electron number i and Φ_{e} is the potential of all electrons.

2.6. Electromagnetic potential and field of a CP

The electric potential of a CP splits as follows:

$$\Phi = \Phi_{\mathrm{n}} + \Phi_{\mathrm{e}} + \Phi_{\mathrm{h}}, \tag{22}$$

where Φ_{n} is the electric potential of the nuclear jellium in the core according to simplification (g), Φ_{e} is the electric potential of the electrons, and Φ_{h} is the electric potential of the halo (44).

The charge density of a CP splits as follows:

$$\bar{\sigma}\left(\rho'\right) = \bar{\sigma}_{\mathrm{n}}\left(\rho'\right) + \bar{\sigma}_{\mathrm{e}}\left(\rho'\right) + \bar{\sigma}_{\mathrm{h}}\left(\rho'\right), \tag{23}$$

i.e., the sum of the nuclear charge density in the core, the electron charge density and the charge density of the halo (43)

The *electric potential* of the CP (in Lorentz gauge, static case) is

$$\Phi\left(\rho\right) = \frac{1}{4\pi\varepsilon_0}\int_0^\infty \bar{\sigma}\left(\rho'\right) G\left(\rho,\rho'\right)\rho'\,\mathrm{d}\rho', \tag{24}$$

where

$$G\left(\rho,\rho'\right) = \begin{cases} 4\pi\left[\ln\left(\bar{L}/2 + \sqrt{\bar{L}^2/4+\rho'^2}\right) - \ln\rho'\right] & \text{for } \rho \le \rho', \\ 4\pi\left[\ln\left(\bar{L}/2 + \sqrt{\bar{L}^2/4+\rho^2}\right) - \ln\rho\right] & \text{for } \rho > \rho'. \end{cases} \tag{25}$$

Replacing $\bar{\sigma}\left(\rho'\right)/\varepsilon_0$ with $\mu_0\bar{J}_z\left(\rho'\right)$ in (24) provides the z-component of the CP's *magnetic vector potential* (in Lorentz gauge, static case):

$$\begin{aligned} \bar{A}_z\left(\rho\right) &= \frac{\mu_0}{4\pi}\int_0^\infty \bar{J}_z\left(\rho'\right) G\left(\rho,\rho'\right)\rho'\,\mathrm{d}\rho' \\ &= -\frac{e\mu_0}{8\pi^2 m_{\mathrm{e}}\bar{L}}\int_0^\infty \sum_{i=1}^{N}\left[\bar{P}_{z,i} + e\bar{A}_z\left(\rho'\right)\right]\left|\Psi_{\rho',i}\right|^2 G\left(\rho,\rho'\right)\rho'\,\mathrm{d}\rho', \end{aligned} \tag{26}$$

where μ_0 is the vacuum permeability, $\bar{J}_z\left(\rho'\right)$ is the z-component of the current density and $\bar{P}_{z,i} = \hbar k_i$ is the z-component of the electron's canonical momentum.

Note that $\bar{A}_z$is depending on itself in Eq. (26). Therefore, the values of $\bar{A}_z$ and $\bar{J}_z$ need to be determined iteratively until self-consistency. Based on the circular boundary condition, (7) the electric potential (24) and the vector potential (26) are made constant in z-direction. This approximation is required for maintaining the full cylindrical symmetry of the model.

The radial and azimuthal (see simplification (m)) components of the vector potential and the current density are zero everywhere. Due to simplification (o) the nuclear jellium is not contributing to the current density. The *radial electric field* of a CP computes as

$$\varepsilon_\rho = -\frac{\partial}{\partial\rho}\Phi\left(\rho\right). \tag{27}$$

The *azimuthal magnetic field* of a CP computes as

$$B_\phi = -\frac{\partial}{\partial\rho}\bar{A}_z\left(\rho\right). \tag{28}$$

2.7. Product ansatz

The following *product ansatz* is made to factorize the electron wave function:

$$\Psi(\rho,\phi,z)=\Psi_\rho(\rho)\,\Psi_\phi(\phi)\,\Psi_z(z)\quad\text{or in short :}\quad\Psi=\Psi_\rho\Psi_\phi\Psi_z. \tag{29}$$

The wave function of a single electron is supposed to be normalized and it represents a stationary state. In azimuthal direction and in axial direction the electromagnetic potential is constant. Therefore, the modulus square of Ψ_ϕ and Ψ_z is also constant:

$$|\Psi_\phi|^2=\Psi_\phi^*\Psi_\phi=\frac{1}{2\pi}\quad\text{and}\quad|\Psi_z|^2=\Psi_z^*\Psi_z=\frac{1}{\bar{L}}. \tag{30}$$

Hence the *modulus square* of the entire wave function factorizes as

$$|\Psi|^2=\Psi_\rho^*(\rho)\,\Psi_\rho(\rho)\,\Psi_\phi^*(\phi)\,\Psi_\phi(\phi)\,\Psi_z^*(z)\,\Psi_z(z)=\frac{1}{2\pi\bar{L}}\,|\Psi_\rho(\rho)|^2\,. \tag{31}$$

The *normalization criteria* (11) could then be carried out as

$$1=\|\Psi\|=\int_0^\infty|\Psi_\rho(\rho)|^2\rho\,\mathrm{d}\rho. \tag{32}$$

2.8. Separation of the Klein–Gordon equation

The following *wave function is solving the z-dependent part* of (29):

$$\Psi_z=\sqrt{\frac{1}{\bar{L}}}\,\mathrm{e}^{ikz},\quad\text{where}\quad k\in\mathbf{R}. \tag{33}$$

Due to simplification (e) the energy eigenvalues are quantized to a discrete spectrum, because wave number k has to meet the following boundary condition:

$$k=l\frac{2\pi}{\bar{L}}, \tag{34}$$

where integer l acts as an *axial quantum number.*

The following *wave function is solving the φ-dependent part* of (29):

$$\Psi_\phi=\sqrt{\frac{1}{2\pi}}\,\mathrm{e}^{im\phi}, \tag{35}$$

where integer m is the *azimuthal quantum number*

Inserting Eqs. (17), (29), (33) and (35) into Eq. (7) provides the *radial Klein–Gordon equation* of a CP:

$$\left\{\frac{\hbar^2}{2m_\mathrm{e}}\left[-\frac{1}{\rho}\frac{\mathrm{d}}{\mathrm{d}\rho}\left(\rho\frac{\mathrm{d}}{\mathrm{d}\rho}\right)+\frac{m^2}{\rho^2}\right]+\frac{\bar{p}_z^2}{2m_\mathrm{e}}-\frac{m_\mathrm{e}c^2}{2}\left(\frac{\bar{E}+e\Phi}{m_\mathrm{e}c^2}+1\right)^2+\frac{m_\mathrm{e}c^2}{2}\right\}\Psi_\rho=0. \tag{36}$$

At the *non-relativistic limit* Eq. (36) becomes the *radial Schrödinger equation* of a CP:

$$\left\{\frac{\hbar^2}{2m_\mathrm{e}}\left[-\frac{1}{\rho}\frac{\mathrm{d}}{\mathrm{d}\rho}\left(\rho\frac{\mathrm{d}}{\mathrm{d}\rho}\right)+\frac{m^2}{\rho^2}\right]+\frac{\bar{p}_z^2}{2m_\mathrm{e}}-\bar{E}-e\Phi\right\}\Psi_\rho=0. \tag{37}$$

The eigenstates of differential equation (36) or (37) provide the radial wave functions Ψ_ρ. The eigenvalues $\bar{E}$ of bound states are discrete, i.e. they are countable by a principal quantum number n, the azimuthal quantum number m and the axial quantum number l. The *principal quantum number* $n = 1, 2, 3, \ldots$ is defined here analogous to the hydrogen atom: n equals one plus the number of node lines of $\Psi_\rho\Psi_\phi$, therefore $n \geq |m| + 1$. (In a stricter sense, Ψ_ϕ has no node lines. However, a standing wave of two superposed azimuthal wave functions, differing only in the sign of quantum number m, has m node lines.)

Principal quantum number n has no explicit representation in (36) or (37) or in any of the following formulas. It is useful however, as an ordering scheme for computational results. One has to keep in mind, that the eigenvalues $\bar{E}$, the eigenstates Ψ_ρ, Ψ_ϕ and Ψ_z, as well as the quantum numbers n, m and l are generally distinct for each electron of the CP. In order to ease readability, the electron number as an index has been omitted from these symbols, unless the index is needed in a summation.

2.9. The jellium model of the nuclear charge distribution

According to simplification (g) the charge of the nuclei is treated as if it were a uniform "positive jelly" background, rather than point charges with distances in between. The nuclear charge density distribution $\bar{\sigma}_\mathrm{n}(\rho)$ of the core jellium has cylindrical symmetry, i.e. it does not depend on φ and z. It is a function of the radial distance ρ.

According to Eqs. (22), (0) and (24) the *electric potential of the core nuclear jellium* is

$$\Phi_\mathrm{n}(\rho)=\frac{1}{4\pi\varepsilon_0}\int_0^\infty \bar{\sigma}_\mathrm{n}(\rho')\,G(\rho,\rho')\,\rho'\,\mathrm{d}\rho'. \tag{38}$$

An infinitesimal charge element $\bar{\sigma}_\mathrm{n}(\rho')\,\rho'\,\mathrm{d}\rho'\,\mathrm{d}\phi\,\mathrm{d}z$ brought into potential Φ_n has the potential energy:

$$\mathrm{d}\bar{E}_\mathrm{n}=\bar{\sigma}_\mathrm{n}(\rho)\,\Phi_\mathrm{n}(\rho)\,\rho\,\mathrm{d}\rho\,\mathrm{d}\phi\,\mathrm{d}z. \tag{39}$$

Integrating (39) over the entire space and dividing the result by two yields the *nuclear self-repulsion energy*:

$$\begin{aligned}\bar{E}_\mathrm{n}&=\bar{E}_\mathrm{n,h}+\bar{E}_\mathrm{h,h}+\frac{1}{2}\int_0^{\bar{L}}\int_0^{2\pi}\int_0^\infty \bar{\sigma}_\mathrm{n}(\rho)\,\Phi_\mathrm{n}(\rho)\,\rho\,\mathrm{d}\rho\,\mathrm{d}\phi\,\mathrm{d}z\\&=\bar{E}_\mathrm{n,h}+\bar{E}_\mathrm{h,h}+\pi\bar{L}\int_0^\infty \bar{\sigma}_\mathrm{n}(\rho)\,\Phi_\mathrm{n}(\rho)\,\rho\,\mathrm{d}\rho,\end{aligned} \tag{40}$$

where $\bar{E}_\mathrm{n,h}$ is the halo-core repulsion energy according to Eq. (46) and $\bar{E}_\mathrm{h,h}$ is the halo self-repulsion energy according to Eq. (47). The division by two in (40) takes care of the fact that the jellium is interacting with itself and the repulsion energy must not be accounted for twice during integration. According to simplification (h) the *nucleic charge distribution in the core* is modeled by means of a two-dimensional distribution function in radial direction.

After studying the computational results of the radial electron density distribution, it became apparent that the charge distribution function can be modeled like this

$$\bar{\sigma}_\mathrm{n}(\rho)=\mathrm{Height}\cdot\exp\left(-\frac{\rho^2}{2\bar{s}^2}-\frac{\rho^5}{\mathrm{Slope}^5}-\frac{\rho^{16}}{\mathrm{Cutoff}^{16}}\right). \tag{41}$$

Parameter Height has to be computed such that the distribution function (41) is normalized to the core nuclear charge Q. Parameters Slope and Cutoff should be adjusted, such that the total energy of the CP is minimized.

2.10. The CP halo (i.e. the charge compensation layer)

The computational results achieved with the cylindrical model show that the core of a CP can carry excess negative charge (e.g. 2% more electrons than nuclear charges). Typically, the surplus negative charge of the CP has to be compensated by a surrounding layer of cations. This layer contains room charge, which terminates the electrical field around the CP core. Throughout this document the charge compensation layer of cations is designated as the "halo" of the CP, whereas the nuclei and the electrons comprising the CP (without the halo) is designated as the "core" of the CP. The halo can also be modeled as a jellium, like the core. If the halo is fully compensating the charge of the core, the *linear charge density of the halo* is

$$\bar{\lambda}_{\mathrm{h}} \equiv \frac{Q_{\mathrm{h}}}{\bar{L}} = -\bar{\lambda}_{\mathrm{e}} - \bar{\lambda}_{\mathrm{n}}, \tag{42}$$

where Q_{h} is the total charge of the halo, $\bar{\lambda}_{\mathrm{n}} = Q/\bar{L}$ is the linear charge density of the nuclei in the core and $\bar{\lambda}_{\mathrm{e}}$ is the linear charge density of the electrons in the core. For the purpose of computing the electric potential in the core, the easiest way is to assume a homogeneously charged cylindrical shell with a radius ρ_{h}, which is larger than the radial extent of the electron orbits and the extent of the nuclear charge distribution of the core (simplification (i)). The shell shall be concentric to the z-axis and have an infinitesimal wall thickness of $\delta\rho$. The *charge density of the halo* cations then is

$$\bar{\sigma}_{\mathrm{h}} = \frac{\bar{\lambda}_{\mathrm{h}}}{2\pi\rho_{\mathrm{h}}\,\delta\rho}. \tag{43}$$

The potential summands sourced by the nuclei and the electrons had been specified in Eq. (22). The *contribution of the halo to the Coulomb potential* computes as

$$\Phi_{\mathrm{h}} = \frac{1}{4\pi\varepsilon_0}\int_0^{\infty} \bar{\sigma}_{\mathrm{h}}\left(\rho'\right) G\left(\rho,\rho'\right)\rho'\,\mathrm{d}\rho' = \frac{\bar{\lambda}_{\mathrm{h}}}{8\pi^2\varepsilon_0}\int_{\rho_{\mathrm{h}}}^{\rho_{\mathrm{h}}+\delta\rho}\frac{1}{\rho'\delta\rho}G\left(\rho,\rho'\right)\rho'\,\mathrm{d}\rho' = \frac{\bar{\lambda}_{\mathrm{h}}}{8\pi^2\varepsilon_0}G\left(\rho_{\mathrm{h}},\rho_{\mathrm{h}}\right). \tag{44}$$

The *contribution of the halo to the Coulomb energy of a single electron* is

$$\bar{E}_{\mathrm{C,h}} \equiv -e\Phi_{\mathrm{h}} = -\frac{e\bar{\lambda}_{\mathrm{h}}}{8\pi^2\varepsilon_0}G\left(\rho_{\mathrm{h}},\rho_{\mathrm{h}}\right). \tag{45}$$

The additional charge of the halo increases the self-repulsion energy between the nuclear charges, as mentioned in Eq. (40). In particular: The *core-halo repulsion energy* can be computed via:

$$\bar{E}_{\mathrm{n,h}} = Q\Phi_{\mathrm{h}}. \tag{46}$$

The *halo self-repulsion energy* is

$$\bar{E}_{\mathrm{h,h}} = \frac{1}{2}Q_{\mathrm{h}}\Phi_{\mathrm{h}}. \tag{47}$$

The result in the above equation was divided by two, because the halo charges are interacting with themselves.

2.11. Approximate solution of the radial wave function

The following *ansatz* will be used for approximating the *radial wave function*:

$$\rho_0 \Psi_\rho \equiv R(r) = f(r) \cdot \exp(-\zeta r), \tag{48}$$

where $r \equiv \rho/\rho_0$ is the relative radius, $\rho_0 \equiv a_0/\sqrt{\lambda_{\mathrm{n}}}$ is the reference radius, $f(r)$ is assumed to be a polynomial and $\zeta \in \mathbf{R}^+$ is a tunable scaling factor.

The value of the *exponential scaling factor* ζ can be determined by analyzing the asymptotic behavior of the wave function R at $r \to \infty$

$$\zeta = \sqrt{\frac{1}{\lambda_{\mathrm{n}}}\left(P_z^2 - \alpha^2 E^2 - 2E\right)}. \tag{49}$$

Therefore,

$$E = \frac{1}{\alpha}\sqrt{P_z^2 - \lambda_{\mathrm{n}}\zeta^2 + \frac{1}{\alpha^2}} - \frac{1}{\alpha^2},$$

where $\lambda_{\mathrm{n}} \equiv Q a_0/e\bar{L}$ is the linear nuclear charge density of the core in natural units, $E \equiv \bar{E}/\bar{E}_{\mathrm{h}}$, $\bar{E}_{\mathrm{h}} \equiv \hbar^2/m_{\mathrm{e}} a_0^2$ is the Hartree energy, $\alpha \equiv \hbar/m_{\mathrm{e}} c a_0$ is the fine structure constant and $P_z \equiv a_0 \bar{P}_z/\hbar$ is the axial canonical momentum of the electron in natural units

At the *non-relativistic limit* the *exponential scaling factor* computes as

$$\zeta = \sqrt{\frac{1}{\lambda_{\mathrm{n}}}\left(P_z^2 - 2E\right)}, \tag{50}$$

thus

$$E = \frac{1}{2}\left(P_z^2 - \lambda_{\mathrm{n}}\zeta^2\right).$$

Inserting (48) and (49) into radial Klein–Gordon equation (36) leads to:

$$\begin{aligned} &-\frac{\lambda_{\mathrm{n}}}{2} f'' + \frac{\lambda_n}{2}\left(2\zeta - \frac{1}{r}\right) f' \\ &+ \left[\frac{\lambda_{\mathrm{n}}\zeta}{2r} + \frac{\lambda_{\mathrm{n}} m^2}{2r^2} + \frac{p_z^2}{2} - \frac{\alpha^2}{2}\left(\frac{1}{\alpha}\sqrt{P_z^2 - \lambda_{\mathrm{n}}\zeta^2 + \frac{1}{\alpha^2}} - E_{\mathrm{C}}\right)^2 + \frac{1}{2\alpha^2} - \frac{\lambda_{\mathrm{n}}\zeta^2}{2}\right] f = 0, \end{aligned} \tag{51}$$

where $E_{\mathrm{C}} \equiv -e\Phi/\bar{E}_{\mathrm{h}}$ is the Coulomb energy in natural units and $p_z \equiv a_0 \bar{p}_z/\hbar$ is the axial kinetic momentum in natural units

For the non-relativistic limit the Schrödinger equation (37) leads to:

$$-\frac{\lambda_{\mathrm{n}}}{2} f'' + \frac{\lambda_{\mathrm{n}}}{2}\left(2\zeta - \frac{1}{r}\right) f' + \left(\frac{\lambda_{\mathrm{n}}\zeta}{2r} + \frac{\lambda_{\mathrm{n}} m^2}{2r^2} - P_z A_z + \frac{A_z^2}{2} + E_{\mathrm{C}}\right) f = 0. \tag{52}$$

Solutions to differential equation (51) or (52) consist of eigenvalues of ζ and eigenstates of polynomial f. These solutions can then be used to compute the eigenvalues of $\bar{E}$ and eigenstates of Ψ_ρ of the radial Klein–Gordon equation (36) or Schrödinger equation (37).

Function $f(r)$ can be *approximated by a polynomial* of r as follows:

$$f(r) \approx \sum_{j=0}^{J} c_j r^{|m|+j} \quad \text{for} \quad c_j \in \mathbf{R} \tag{53}$$

Generally, constants c_j and ζ are depending on quantum numbers n, m and l. For simplicity reasons, this dependency is not reflected in the respective indices of these constants.

In Eq. (57) a number of *terms can be approximated by a polynomial* of degree P:

$$\frac{p_z^2}{2} - \frac{\alpha^2}{2}\left(\frac{1}{\alpha}\sqrt{P_z^2 - \lambda_{\mathrm{n}}\zeta^2 + \frac{1}{\alpha^2}} - E_{\mathbf{C}}\right)^2 + \frac{1}{2\alpha^2} - \frac{\lambda_{\mathrm{n}}\zeta^2}{2} \approx \sum_{p=0}^{P} b_p r^p, \tag{54}$$

where $P \leq J-1$ and $b_p \in \mathbf{R}$

At the non-relativistic limit (54) simplifies to:

$$-P_z A_z + \frac{A_z^2}{2} + E_{\mathbf{C}} \approx \sum_{p=0}^{P} b_p r^p, \tag{55}$$

where $P \leq J-1$ and $b_p \in \mathbf{R}$

A good approximation accuracy has been achieved with $P = 8$. The *coefficients* c_j can be computed by *the iterative formula* from the value of c_0:

$$c_j = \frac{1}{(2|m|j + j^2)}\left\{\zeta(2|m| + 2j - 1)c_{j-1} + \frac{2}{\lambda_{\mathrm{n}}}\sum_{p=0}^{P} b_p c_{j-p-2}\right\}, \tag{56}$$

where $c_i = 0$ for $i < 0$

Note, that the coefficients c_j are all proportional to each other. Formula (56) stays the same at the non-relativistic limit. The last coefficient c_J is zero, only in case ξ is an *eigenvalue*. All eigenvalue can be found this way. The *value of coefficient* c_0 can be determined from ζ by normalization of the wave function R. The normalization condition (32) requires:

$$1 = \|R\| = \int_0^\infty |R(r)|^2 r\,\mathrm{d}r = \int_0^\infty \left(\sum_{j=0}^{J} c_j r^{|m|+j}\right)^2 \exp(-2\zeta r)\, r\,\mathrm{d}r. \tag{57}$$

That means, one has to scale all c_j proportionally, such that (57) yields the value 1.

2.12. Grouping, orbital occupation, self-consistent field iterations

The electron configuration of a CP consists of many orbitals, which are characterized by the quantum numbers n, m and l. According to the Pauli Exclusion Principle each orbital can only be occupied by a maximum of two electrons (one with spin up and one with spin down).

There are too many electrons in a CP to compute all occupied orbitals individually. Instead, ranges of orbitals with contiguous values for l are grouped together. Within a group all orbitals have the same quantum numbers n and m. These orbitals of such groups differ in quantum number l. The arithmetic mean of the quantum numbers l represents the group during computation. Equations (14) and (16) are computed by letting the summation run over the occupied number of groups. Each summand is multiplied by the number of electrons it represents. For ground state computations of the occupation should start with the lowest energy. It should progress to groups with successively higher energy until the targeted number of electrons "found their orbital".

Equations (14), (16) and (56), as well as the occupation process are depending on each other in a circular manner. Thus, they can be computed only *iteratively* until reaching *self-consistency between eigenstates, potential and occupation*. Within each of these SCF-iterations (self-consistent field iterations) there is a need for sub-iterations:

According to (16) and (26) the axial current density J_z and the vector potential A_z are mutually dependent on each other. Sub-iterations are required for making these quantities consistent with each other, while leaving the eigenstates unchanged.

3. Computational Results from the Cylindrical Model

3.1. The physical properties of the "Golden Configuration"

The author has programmed a "simulator" tool [17], which implements the mathematics of the cylindrical model described in Section 2. Many different configurations of CPs have been simulated successfully with this tool. In the current section, only one of these configurations will be described, which the author believes is among the most stable ones. This configuration is called the "golden configuration" throughout this document.

The golden configuration of a CP is characterized by the following *input parameters*:

- The computation was relativistic, i.e. the Klein–Gordon equation was engaged.
- A template with 14 750 orbital groups was used. The template specifies the quantum numbers n, m and l for groups of electrons. The orbitals (i.e. eigenvalues and eigenstates) of these groups were calculated as candidates for occupation. 7375 of these groups were actually occupied in the order of the computed eigenvalues.
- The length of the CP was set to 9.6 mm.
- The nuclei in the jellium had a mean charge of 48 elementary charges.
- The linear charge density of the nuclei $\lambda_{\mathbf{n}}$ was set to 500 elementary charges per picometer length of the CP.
- The number of electrons was set to be 102% of the total number of elementary charges contained in all the core nuclei combined.
- A halo of cations was configured to reside at a distance of $150\rho_0 = 48.8\,\text{pm}$, such that the total charge of the CP is zero (neutral).
- The core nuclear charge distribution was computed according to Eq. (60) with a standard deviation of $\bar{s} = 90\rho_0 = 29.3\,\text{pm}$, a slope parameter of Slope $= 105\rho_0 = 34.2\,\text{pm}$ and a cutoff parameter of Cutoff $= 115\rho_0 = 37.4\,\text{pm}$.
- The maximum number of coefficients c_j of the wave function polynomial was set to 2150.
- The axial velocity of the electrons was limited to $10\% \leq v_z \leq 80\%$ of the speed of light.

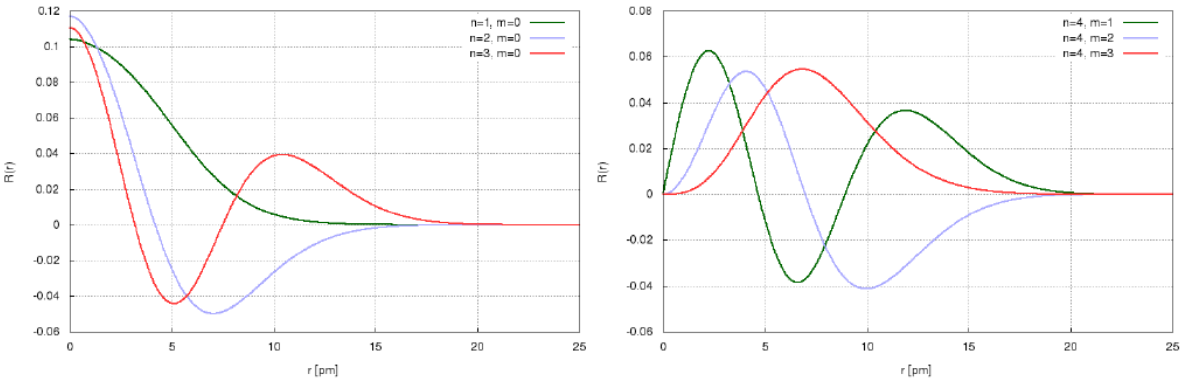

Figure 7. Plots of three radial wave functions $R(r)$ against the radius r; *Left*: With principle quantum numbers $n = 1, 2$ and 3 and azimuth quantum number $m = 0$. *Right*: With principle quantum numbers $n = 4$ and azimuth quantum number $m = 1, 2$ and 3.

The simulator tool in this case had to compute 44 iterations before reaching a self-consistent field status, where the field of the electron charge distribution was self-consistent with the eigenstates of the occupied groups. The tool lists the resulting eigenvalues (in eV) of the groups ordered by their quantum number in a huge triangular table.

The eigenvalues within a single field of the table are distinguished by quantum number l, i.e. the electrons of the respective groups have different axial velocities. Each eigenvalue has a hyperlink, which upon clicking opens a detailed description of the respective eigenstate, including a plot of the wave function. Plots with samples of the computed wave functions are shown in Fig. 7:

As can be seen from Fig. 7, the number of zeros of the wave functions equals $n - m$, whereby the last zero is at infinite radiuses. The radial extent of the wave functions generally increases with principal quantum number n. The eigenvalues of wave functions with identical n and l but different m are non-degenerate (i.e. they are different): The

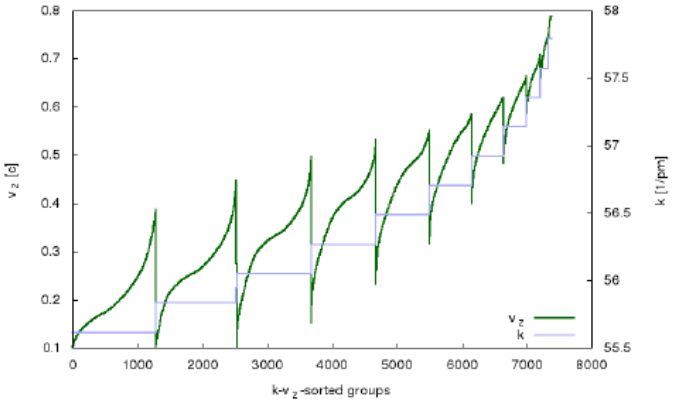

Figure 8. Distributions of the electron's axial velocities (v_z) and axial wave numbers (k). The occupied groups have been sorted at first by wave number. Within the ranges of constant wave numbers the groups have then been sorted by velocity.

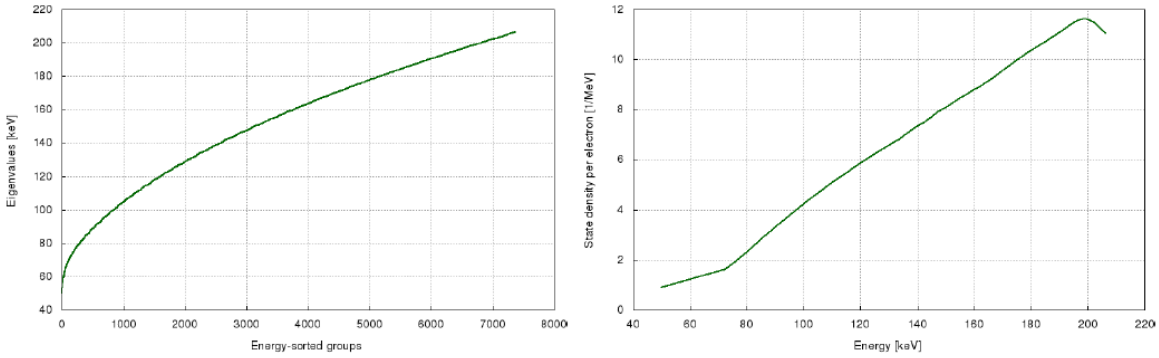

Figure 9. *Left*: Electron eigenvalue distribution. The occupied groups have been sorted by energy eigenvalue; *Right*: Electron state density distribution. It has been computed by exchanging the x and y axes of the left figure and then forming the first derivative via numerical derivation. The state density measures, how many quantum states per electron exist in an infinitesimal energy interval.

radial extent of a wave function (with a fixed n) decreases and the eigenvalue decreases with increasing m.

The symmetry of the axial velocity distribution is broken, i.e. it is not centered symmetrically on zero. The axial velocity correlates with the wave number of the axial de Broglie waves. The wave number distribution is also asymmetric. Both distributions can be seen in Fig. 8:

- The total nuclear charge of the CP core is 7.69 $\times 10^{-7}$ C.
- The total charge of the halo cations is an additional 1.54×10^{-8} C.
- The CP contains 100 billion nuclei.
- There are 4.90×10^{12} electrons in the CP.
- Each electron group contains 664 million electrons.
- The maximum matter density in the CP core is 647 kg/cm^3 for cadmium, 92.0 kg/cm^3 for oxygen and 5.80 kg/cm^3 for hydrogen. For cadmium this is about 75,000 times denser than ordinary metal.

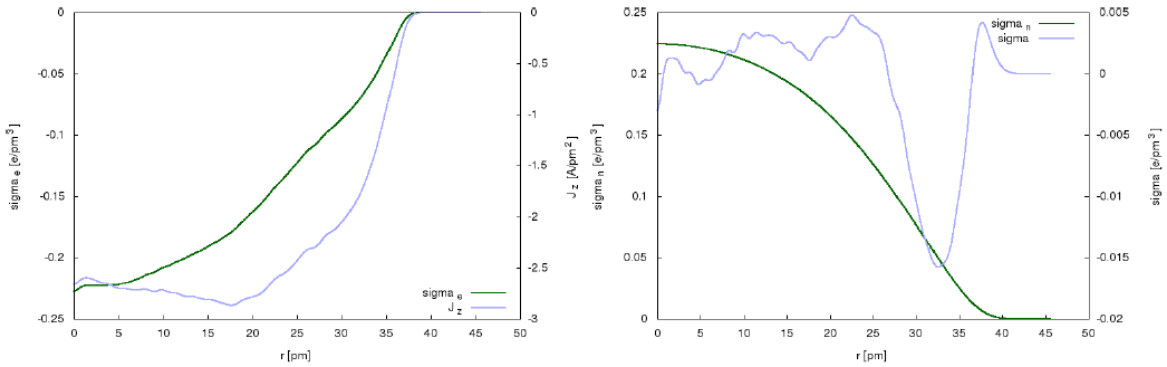

Figure 10. *Left*: Radial distributions of the electron charge density (σ_e) and the current density (J_z). *Right*: Radial Distributions of the core nuclear charge density (σ_n) versus the total charge density (σ).

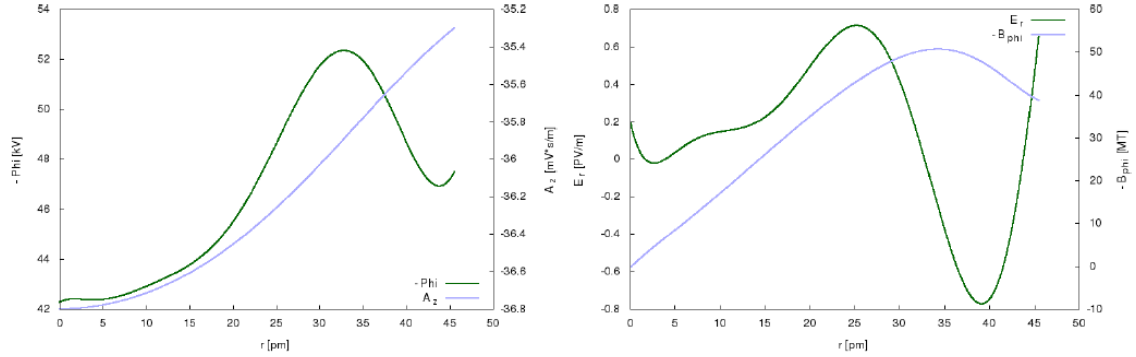

Figure 11. *Left*: Electric potential (φ) and magnetic potential (A_z). *Right*: Radial electric field (E_r) and azimuthal magnetic field ($B\varphi$).

- The kinetic energy of the electrons ranges from 1.9 to 155 keV, stemming mostly from the axial movement
- The axial de Broglie wavelength of the electrons ranges from 0.108 to 0.113 pm

3.2. Varying the input parameters

The most prominent changes of the simulation results occur when the linear charge density of the core λ_n is varied. The total number of nuclei and electrons in the CP has been kept constant for this comparison: Other key properties of a CP also change significantly, when the linear charge density of the core nuclei λ_n is varied (Table 1):

Varying λ_n strongly changes the eigenvalue distribution: The minimum axial velocity also has strong influence on the properties of the CP, mainly because it changes the axial current of the CP: Varying the minimum axial velocity is changing the eigenvalues, because of the differences in the axial kinetic energy. Other key properties changing with the minimum axial velocity are as follows (Table 2).

The staircase shape of the wave number graph is an artifact from electron grouping: A whole range of wave numbers is represented by its mean value of the group. With a larger number of groups in the simulation template, the

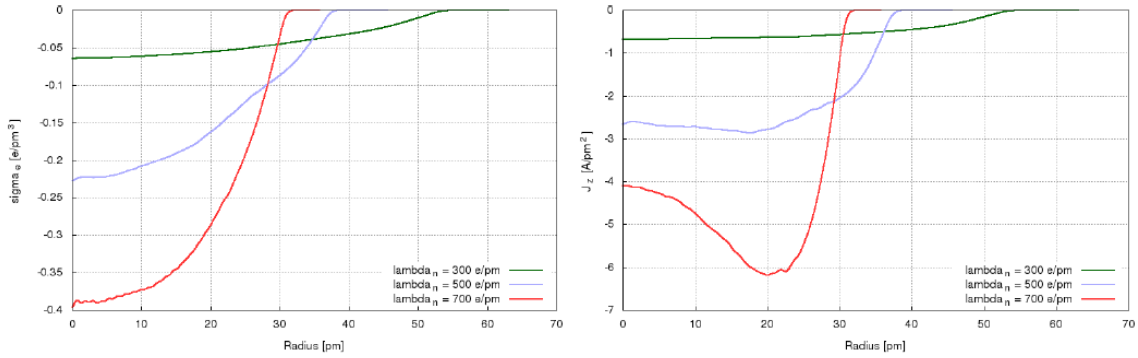

Figure 12. Electron charge density distribution (*top*) and current density distribution (*bottom*) at different values for the linear charge density λ_n of the nuclei.

Table 1. Changes of key properties, when the linear charge density of the core nuclei λ_n is varied (the "golden configuration" is marked bold).

Linear charge density of the core (e/pm)	100	200	300	400	**500**	600	700	800
CP length (mm)	48	24	16	12	9.6	8	6.86	6
Reference radius (pm)	0.727	0.514	0.420	0.364	0.325	0.297	0.275	0.257
Mean expectation value of the electron radius (pm)	66.2	39.6	29.2	23.7	20.2	17.8	17.0	16.3
Mean expectation value of the electron charge density (e/pm^3)	–0.0029	–0.0159	–0.0433	–0.0875	–0.150	–0.231	–0.297	–0.374
Mean expectation value of the current density (A/pm^2)	–0.0222	–0.160	–0.529	–1.24	–2.48	–4.06	–5.26	–6.81
Formation energy per electron (keV)	9.79	24.4	43.4	65.2	92.3	118	136	158
Min. electric potential of the core (kV)	–7.36	–18.3	–27.9	–39.5	–52.3	–60.7	–66.6	–79.6
Total axial current (kA)	–0.779	–2.08	–3.90	–6.15	–9.21	–12.0	–14.2	–16.7
Mean axial velocity (c)	0.159	0.213	0.265	0.314	0.376	0.409	0.414	0.426
Max. magnetic flux density (MT)	1.43	6.24	15.3	29.3	50.7	74.8	94.6	119
Characteristic Impedance (Ω)	653	673	684	692	698	703	705	706
Inductance (nH)	165	85.1	57.7	43.8	35.3	29.7	25.5	22.4
Capacitance (fF)	388	188	123	91.5	72.5	60.0	51.4	44.8
Magnetic flux (μWb)	129	177	225	269	326	356	362	373
Energy of the magnetic flux per electron (MeV)	0.0639	0.235	0.560	1.06	1.91	2.72	3.28	3.98
Minimum nuclear distance (Z_m =48, 8 and 1) (pm)	27.8	15.7	11.2	8.80	7.42	6.52	6.16	5.83
	15.3	8.64	6.16	4.84	4.08	3.59	3.39	3.21
	7.65	4.32	3.08	2.42	2.04	1.79	1.69	1.60
Lowest occupied orbital eigenvalue (keV)	8.35	15.5	22.9	28.5	49.9	58.3	72.4	87.3
Highest occupied orbital eigenvalue (keV)	26.4	61.5	102	147	206	258	298	350
Max. state density per electron (1/MeV)	114	42.9	25.7	18.2	11.6	8.83	7.56	6.03

steps get smaller. The velocity ranges for neighboring wave number values are overlapping, which results in the saw teeth shape of the velocity distribution graph. The energy eigenvalues of the occupied orbitals is distributed according to Fig. 9. The charge density distribution and the current density distribution computed as follows.

At radius values around 32 pm the electron charge density exceeds the nuclear charge density. The resulting total charge density distribution can be seen at the right side of Fig. 10. The electric and magnetic potentials, as well as the electric and magnetic fields as a function of the radius is shown here.

Other computation results for the golden configuration are listed in column "500" in Table 1. Additionally, the following values have been computed. The following diagrams compare the results of non-relativistic simulations (via the Schrödinger equation) with relativistic simulations (via the Klein–Gordon equation).

As can be seen above, there is virtually no difference in the electron charge distributions for both types of simulation runs. The same is true for the individual wave functions. However, the eigenvalue distribution changes markedly

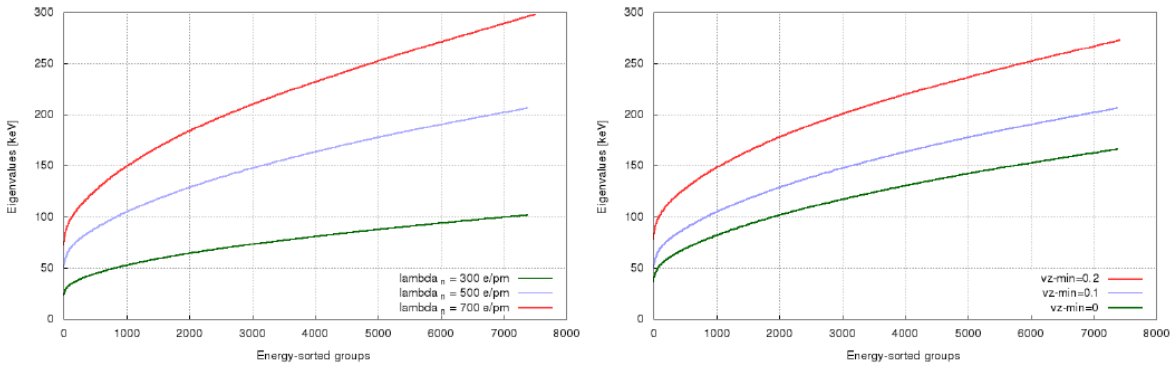

Figure 13. *Top*: Changes of the eigenvalue distribution, when λ_n is varied. *Bottom*: Changes of the eigenvalue distribution, when the minimum axial velocity is varied.

between non-relativistic versus relativistic simulations. These changes lead to a higher (i.e. more endothermic) formation energy and a lower state density at non-relativist runs. Except for the purpose of this comparison here, all properties of CPs were obtained by relativistic simulations. The length of a CP and the number of electrons in the CP core have only minor influence on the resulting properties. Therefore, no details are shown here.

3.3. Confinement, stability, formation energy, electron scattering

According to Fig. 11 the electric potential in the CP core is below –47.5 keV with an electron surplus of 2% against the nuclear charges. The potential is repulsive to the electrons and attractive to the nuclei. *The electric potential safely confines/traps the nuclei* inside the core. The negative potential is a direct result of the electron surplus in the CP core. The larger this surplus is, the more negative the potential will become. It is believed that there is an equilibrium of diffusion for the nuclei: If the core potential is becoming too negative, nuclei from the surrounding matter will be pulled into the core. If the core potential is becoming less negative, nuclei from the core will diffuse out and will

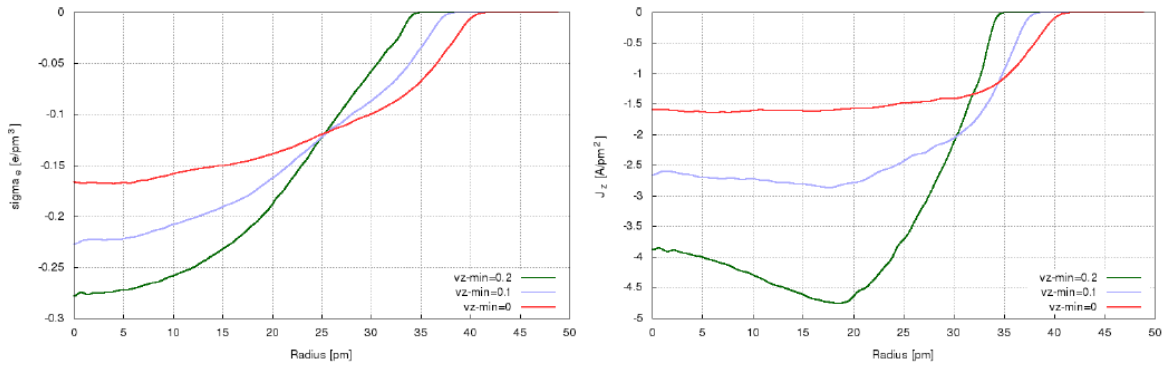

Figure 14. Electron charge density distribution (*left*) and current density distribution (*right*), at different values of the minimum axial velocity (in units of the light speed) of the electrons.

Table 2. Changes of key properties, when the minimum of the axial velocity of the electrons is changed is varied.

	$v_{z,\min} = 0$	$v_{z,\min} = 0.1{\cdot}c$	$v_{z,\min} = 0.2{\cdot}c$
Formation energy	66.1 keV	92.3 keV	132 keV
Total axial current	–6.38 kA	–9.21 kA	–12.2 kA
Mean axial velocity	0.260 c	0.376 c	0.498 c
Mean expectation value of the electron radius	22.7 pm	20.2 pm	18.0 pm
Mean expectation value of the electron charge density	–0.120 (e/pm^3)	–0.150 (e/pm^3)	–0.190 (e/pm^3)
Mean expectation value of the current density	–1.43 (A/pm^2)	–2.48 (A/pm^2)	–4.05 (A/pm^2)
Min. electric potential of the core	–48.5 kV	–52.3 kV	–63.3 kV
Max. magnetic flux density	–32.6 MT	–50.7 MT	–74.4 MT
Minimum nuclear distance (Z_m =48)	8.15 pm	7.42 pm	6.92 pm
Lowest occupied orbital eigenvalue	36.9 keV	49.9 keV	78.1 keV
Highest occupied orbital eigenvalue	166 keV	206 keV	273 keV

recombine with electrons from the surrounding matter. A quantitative analysis of this equilibrium is not available, however.

The magnetic potential confines the electrons in radial direction safely, because the axial velocity of the electrons is in positive z-direction. Therefore, the electrons will be compressed against the z-axis (z-pinch). The confinement of the electrons in axial direction exists only, if the CP has formed a *closed loop*, i.e. the electrons cannot escape at the ends. In open-ended configurations of a CP, the electrons will be emitted at one end of the CP, while the other end will be depleted from electrons. It is clear, that open-ended CP configurations are not stable. However, they can exist in a transient manner, e. g. while being attached to a cathode and in the presence of a strong electric field. The cathode in this case has to replace the electrons at the positive end of the CP, at the same rate the electrons are emitted at the negative end. Within the current framework of the cylindrical model the *length stability of a CP* remains enigmatic. In consequence it is uncertain at which densities CPs are most stable. On one hand, there is ample experimental evidence available showing that CPs are either energetically metastable or dynamically stable with lifetimes sometimes exceeding one hour. On the other hand, a CP with the binding energies according to Table 1 would just elongate itself and decay, because the binding energies fall monotonically with the CP length.

Could the length stability be caused by a yet unknown term of the Hamiltonian, which lowers the formation energy at higher densities? Arguments exist as to why the resistive losses in a CP at low or moderate temperatures are expected to be extremely small: Small-angle scattering of the electrons would need to occupy higher-energy orbitals or would

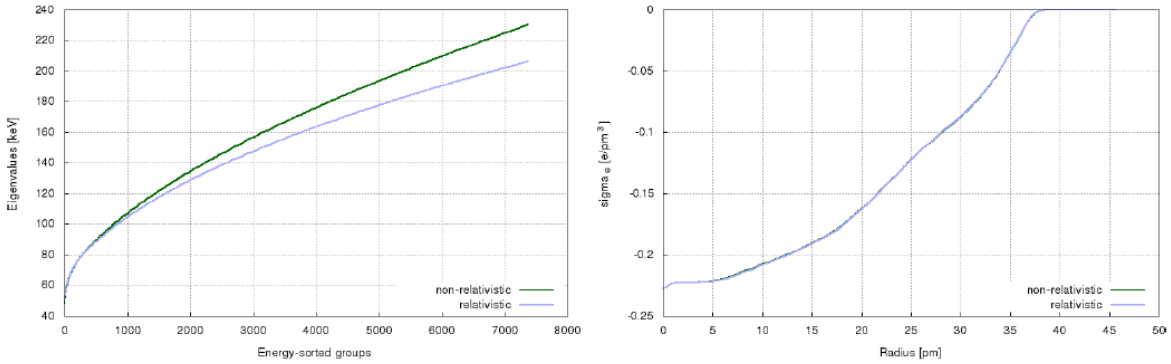

Figure 15. Eigenvalue distribution and electron charge density distribution, non-relativistic versus relativistic.

result in orbitals, which are already occupied. Thus, one can say that small-angle *scattering is* quantum mechanically *suppressed.*

Large-angle scattering (such as the reflection of electrons by the core nuclei) is also suppressed, because the resulting orbitals would run in negative z-direction. The resulting eigenvalues would be higher than before the reflection, i.e. the reflection will not occur. Only at very high temperatures (above hundreds or thousands Kelvin) will there be sizable electron-phonon scattering (both, small-angle and large-angle). Some of the resulting eigenstates will have negative axial velocities. These electrons will be repelled from the CP by the electric field (i.e. they will be lost). In other cases, the resulting eigenstates will relax back (under electromagnetic radiation) to the lower-energy eigenstates, which were populated before the scattering occurred.

Interestingly, the electrons, which will be accelerated in positive z-direction, cannot relax back to lower velocities, because linear movement of charges does not radiate. In effect, very high temperatures in the core can increase the mean axial velocity of the electrons. In order for the model proposed here to account for stable CPs, the resistive loss will need to be very low. The reasons given above are thought to be plausible as to how this might come about. However, further analysis or experimentation is required for clarification.

If the resistive losses are indeed very small, the magnetic flux of a CP is expected to be virtually constant in a sub-millisecond timeframe. Over a longer time span the flux can potentially change slowly (in both directions, depending on the external conditions). For a CP to decay, the axial movement of the electrons has to slow down. This, however, takes a long time because of the said lack of electron scattering and because the magnetic flux can change only very slowly.

4. Summary and Conclusions

Previously known as "strange radiation", a novel aggregation state of matter has been characterized and named "condensed plasmoids" (CP). A quantum-mechanical model of CPs was built, a computer program was designed, and computer calculations were used to obtain the properties of CPs. The computed properties are well-aligned with many experimental findings in LENR, including the strange patterns left by CPs on the surfaces of electrodes and x-ray films.

CPs compress matter magnetically to such high densities that atomic nuclei can tunnel through the Coulomb barrier, thereby enabling fusion. The current modeling is seen as being incomplete, because no length stability of CPs was found and because the calculated intrinsic current of CPs appears to be larger than what can be concluded from the experiments. This is probably caused by inaccuracies in the relativistic Hamiltonian.

Hopefully, the theory on CPs will reinvigorate the scientific discourse between research groups, startup companies and other organizations, which lately were working on their patents and LENR reactor designs in an understandably closed-lipped fashion. Without an open scientific dialogue on CPs however, the completion of this theory cannot be achieved. Hopefully, the theory on CPs will be instrumental in the technical development of *reliable, durable and safe* LENR reactors and timely commercialization.

References

[1] Lutz Jaitner, *The Physics of Condensed Plasmoids and Low-Energy Nuclear Reactions (LENR)*, comprehensive article at the author's web site, 2015–2019,
http://condensed-plasmoids.com/condensed_plasmoids_lenr.pdf.

[2] Claude Daviau, Daniel Fargue, Didier Priem and Gulliaume Racineux, *Tracks of magnetic monopoles*, *Annales de la Fondation Louis de Broglie* **38** (2013),
http://aflb.ensmp.fr/AFLB-381/aflb381m778.pdf.

[3] B. Rodinov and Irina Savvatimova*, Unusual Structures on the Material Surfaces Irradiated by Low Energy Ions*, archived at

LENR-CANR.org,, 2005,
http://www.lenr-canr.org/acrobat/RodionovBunusualstr.pdf.
[4] Takaaki Matsumoto, Bulletin of the Faculty of Engineering, Hokkaido Univ., No. 175, 1995, p. 73.
[5] W.-S. Zhang and J. Dash, Excess heat reproducibility and evidence of anomalous elements after electrolysis in $Pd/D_2O+H_2SO_4$ electrolytic cells, *13th Int. Conf. Condensed Matter Nucl. Sci.*, 2007,
http://www.lenr-canr.org/acrobat/ZhangWSexcessheat.pdf.
[6] A. Klimov et al., Interaction of hydrogen atoms and ions with erosive metal clusters in heterogeneous plasmoid, *12th IWAHLM*, Italy, 2017,
http://www.iscmns.org/work12/KlimovAinteractionof.pdf.
[7] Edmund Storms, *The Nature of the Nuclear-Active-Environment Required for Low Energy Nuclear Reactions*, Submitted to Infinite Energy, 2002,
http://www.lenr-canr.org/acrobat/StormsEthenatureoa.pdf.
[8] W.H. Bennett, Magnetically self-focusing streams, *Phys. Rev*. **45** (1934) 890.
[9] R.S. Pease, Equilibrium characteristics of a pinched gas discharge cooled by bremsstrahlung radiation, *Proc. Roy. Soc. London Ser. B* **70** (1957) 11–13.
[10] S.I. Braginskii, On the behavior of a completely ionized plasma in a strong magnetic field, *Zhur. Eksptl'. i Teoret. Fiz.* **33** (1957) 645.
[11] S.I. Braginskii, Contribution to the theory of spark channels, *Sov. Phys. JETP* **6** (1957) 494–501.
[12] Robert S. Cohen, Lyman Spitzer and Paul McR. Routly, The electrical conductivity of an ionized gas, *Phys. Rev*. **80** (2) (1950) 230–238,
http://ayuba.fr/pdf/spitzer1950.pdf.
[13] K.N. Koshelev and N.R. Pereira, Plasma points and radiative collapse in vacuum sparks, *J. Appl. Phys*. **69**(10) (1991) R21–R44,
https://www.researchgate.net/publication/224546528_Plasma_points_and_radiative_collapse_in_vacuum_sparks.
[14] J. Va'vra, J.A. Maly and P.M. Va'vra, Soft X-ray production in spark discharges in hydrogen, nitrogen, air, argon and xenon gases, SLAC-PUB-7683, *Nucl. Instr. Methods Phys. Res. Section A* **418** (2,3) (1998) 405–419,
https://www.slac.stanford.edu/pubs/slacpubs/7500/slac-pub-7683.pdf
[15] P.W. Atkins, *Molecular Quantum Mechanics*, Parts I and II: *An Introduction to Quantum Chemistry*, Vol. 1, Oxford University Press, Oxford, ISBN 0-19-855129-0, 1977.
[16] Kohn Walter and Sham Lu Jeu, Self-consistent equations including exchange and correlation effects, *Phys. Rev.* **140** (4A) (1965) A1133–A1138.
[17] Lutz Jaitner, *CP Simulator*, online program, 2016–2019,
https://condensed-plasmoids.com/dyn?cmd=retrieve_simulation_form.